Publsihed in International Journal of Electrical Power & Energy Systems with doi:

10.1016/j.ijepes.2022.108493

Comprehensive Enhanced Newton Raphson Approach for Power Flow Analysis in Droop-Controlled Islanded AC Microgrids

Mohammad Bayat[a], Masoud Mehrabi Koushki[a], Ali Asghar Ghadimi[a], Marcos Tostado-Véliz[b], Francisco Jurado[b,*]

[a]Department of Electrical Engineering, Faculty of Engineering, Arak University, Arak 38156-8-8349, Iran
[b]Department of Electrical Engineering, University of Jaén, 23700 EPS Linares, Jaén, Spain

Abstract - One of the essential studies in the operation and planning of a microgrid is the Power Flow (PF). Traditional PF methods are not applicable for droop-controlled islanded microgrids due to the absence of a slack bus in the system, the dependence of the Distributed Generators (DGs) output power to droop characteristics, and the frequency and voltage dependency of loads. In this regard, this paper develops an Enhanced Newton Raphson (ENR) method for PF in the droop-controlled islanded microgrids. The proposed method is based on the well-known NR method but with a more comprehensive model that considers different types of droop schemes (resistive, inductive, and complex), load demand dependency on voltage and frequency, π line model, and shunt compensators. Moreover, a new index for selecting proper droop characteristics for any droop-controlled islanded microgrid is proposed. Five test systems with different scales, different topologies, different droop control strategies and different load models are considered for evaluating the performance of the proposed method. The results are compared with the recently developed methods and the steady-state results of Time-Domain (TD) simulations conducted in PLECS software. The results show that the proposed technique has excellent accuracy with low computational time and can be easily integrated into the currently available power system analysis tools.

Keywords: Power flow, Droop-controlled islanded microgrids, Newton Raphson

---

*Corresponding author, Tel.: +34 953 648518; Fax: +34 953 648586; E-mail: fjurado@ujaen.es

1. Introduction

Power Flow (PF) is the cornerstone of power system analysis computational tools, as it is the basis of many optimizations, control, and security analysis applications, among others [1], [2]. Typically, PF is a set of nonlinear equations that relate the nodal voltages to the nodal power injections. The main result of this set of equations is the steady-state operating point of the system. As a nonlinear problem, PF has been customarily solved using iterative techniques. Among the plethora of nonlinear solvers proposed for solving PF (see Literature Review in [3] and [4]), the Newton Raphson (NR) technique has been, by far, the most widely used technique in industrial tools.

Besides, deregulated power systems have brought a growing interest in Distributed Generators (DGs) in recent years [5] under the concept of microgrid. DGs are able to provide a reliable electricity supply to remote areas that are not directly connected to an upscale grid or have become islanded because of a fault in the network. This emerging paradigm is called islanded microgrid. Even a small islanded microgrid needs power flow calculation for planning and operation purposes, similar to an large power system.

The increasing need for analyzing the islanded microgrids has led to revising the conventional PF tools, which cannot be directly applied to the analysis of these grids. Indeed, conventional PF programs assume the existence of a slack bus (whose voltage magnitude is known) and a constant system frequency. In addition, the bus admittance matrix is assumed to be constant, and buses are customarily classified into PQ and PV classes. Since these assumptions are not usually valid for islanded microgrids [5], multiple works have been recently conducted on developing novel computational tools suitable for PF analysis of islanded microgrids.

Many references have coped with PF analysis of islanded microgrids by treating the system frequency as an extra variable. This approach forces the inclusion of extra

equations within the original system. The resulting system of nonlinear equations is then handled using conventional solvers like the backward/forward sweep algorithm [6]-[8], Trust Region approaches [9], or metaheuristic techniques [10]. Nevertheless, extended NR-based formulations have been preferred for PF analysis of islanded microgrids as contemplated in various references [5], [11]-[14].

Other references have avoided the variable-frequency issue by proposing innovative strategies, such as the references [15] and [16]. These references have proposed an alternative algorithm in which a slack bus is randomly selected among the MG buses; then, the problem is iteratively solved until the power injections in the selected slack bus are zero, indicating the islanded operation mode. Other references have aimed to pose alternative strategies to incorporate conventional methods to PF analysis of islanded microgrids. In [17] and [18], the variability of the bus admittance matrix with respect to frequency is overcome by proposing a single-loop iterative algorithm, in which the current injection form of the PF equations is used [19]. The authors in [20] aimed at extending the applicability of the Backward/Forward Sweep (BFS) algorithm and the conventional PF problem in current injection form to islanded microgrids, by using complex compensation methods. The authors in [21] have recently proposed an efficient iterative approach to reduce the computational time of solving the PF problem in islanded microgrids using conventional methods.

Different operating modes of DGs have been treated for proper power-sharing [22] along with the most typical loop-based control. The reference [23] has also contemplated the isochronous operating mode. When an microgrid is operated under isochronous conditions, a dominant DG acts as a slack bus (i.e., maintaining the frequency and voltage constant at its terminals regardless of the connected load). However, it cannot be

considered as an ideal slack bus as the isochronous generator cannot keep its terminal voltages balanced under unbalanced loads.

Motivated by the aforesaid challenges, and as an extension of the proposed methods in [5] and [12], an Enhanced Newton Raphson (ENR) approach is presented in this paper for solving the PF problem in droop-controlled islanded microgrids. The main contributions of this paper are listed as follows:

- A unified formulation is provided for handling different types of droop-controlled DGs.
- Unlike previous studies that modify the NR approach for a simple network model, microgrid network modeling has been provided in full detail. The effect of parallel elements (including the line capacitors of underground cables and the probable compensators) are considered in the proposed formulation.
- Introducing a novel index named Power Sharing Error Index (PSEI) in order to determine which type of droop control is appropriate for the DCIMG.
- Suitable modeling of droop-controlled islanded microgrid in Time-Domain (TD) simulators is provided, which is adapted for PF studies, including DGs with different types of droop characteristics and different types of frequency and voltage-dependent loads.

The rest of the paper is organized as follows: In Section 2, further modeling of islanded microgrids for PF analysis is developed. Section 3 presents the formulation of the ENR approach, which is adapted for PF analysis of islanded microgrids. In Section 4, the numerical results of the proposed method are validated in comparison with the results of TD simulations conducted by PLECS software. Moreover, the verification of the results against the recently derived approaches is provided in this section. Finally, the conclusions are provided in Section 5.

2. Islanded microgrid modeling for PF analysis

The PF analysis is the foundation of studying the steady-state characteristics of a power grid. This study needs an appropriate model of the system components, which will be discussed in this section for an islanded microgrids.

2.1. Droop-controlled DG model

The droop equation is distinguished based on the output impedance of the DG. If the imaginary part of the output impedance of a DG is greater than its real part, the active and reactive powers are related to frequency and voltage, respectively. This droop type is called the conventional droop or inductive droop. Some distribution networks like cable type or low voltage networks are resistive. Therefore the reactive and active powers are related to the frequency and voltage, respectively. In this case, the droop type is called inverse droop or resistive droop. If they could not get over each other, the droop type is considered a mixed type, and this condition is known as the complex output impedance of DG. In this situation, the active and reactive powers are related to both frequency and voltage. In [17], possible combinations are categorized by two binary variables x and y. Considering this, for the DG unit located in bus i,

$$P_{Gi} = P_{0i} + G_{pfi}(f - f_0) + G_{pvi}(V_i - V_{0i}) \quad (1)$$

$$Q_{Gi} = Q_{0i} + G_{qfi}(f - f_0) + G_{qvi}(V_i - V_{0i}) \quad (2)$$

where

$$\begin{aligned} G_{pfi} &= -\frac{1}{m_i}\left(\frac{x_i}{x_i+y_i}\right), & G_{qfi} &= \frac{1}{m_i}\left(\frac{y_i}{x_i+y_i}\right) \\ G_{pvi} &= -\frac{1}{n_i}\left(\frac{y_i}{x_i+y_i}\right), & G_{qvi} &= -\frac{1}{n_i}\left(\frac{x_i}{x_i+y_i}\right) \end{aligned} \quad (3)$$

In the expressions above, P_{0i}, Q_{0i}, f_0 and V_{0i} are set-points of active power, reactive power, system frequency, and voltage magnitude of bus i, respectively. f and V_i are system frequency and voltage magnitude of bus i. m_i and n_i are frequency droop coefficient and the voltage magnitude droop coefficient, respectively. Different

combinations of x and y in (3) result in different types of droop formulations. Inductive (conventional) with $x = 1$ and $y = 0$, resistive (inverse) with $x = 0$ and $y = 1$, and complex with $x = y = 1$.

2.2. Load model

The demanded active and reactive power of loads in the i^{th} bus, (i.e., P_{Li} and Q_{Li}) can be represented as [24],

$$P_{Li} = P_{Lni}\left(1 + L_{pfi}(f - f_n)\right)\left(\frac{V_i}{V_{ni}}\right)^{L_{pvi}} \quad (4)$$

$$Q_{Li} = Q_{Lni}\left(1 + L_{qfi}(f - f_n)\right)\left(\frac{V_i}{V_{ni}}\right)^{L_{qvi}} \quad (5)$$

where P_{Lni} and Q_{Lni} are active and reactive power demands of loads, respectively, in the nominal operating condition of f_n and V_{ni}. The parameters L_{pvi} and L_{qvi} in the exponential model represent the voltage dependency of P_{Li} and Q_{Li}. Constant power (CP), constant current (CI), and constant impedance (CZ) load models can be expressed by selecting the L_{pvi} and L_{qvi} as 0, 1, and 2, respectively. Moreover, L_{pfi} and L_{qfi} denote the coefficients of frequency dependency of loads.

2.3. Network model

Branches, including feeders and transformers, are expressed by the π model in power flow studies. Using this model, the bus admittance matrix $\overline{\boldsymbol{Y}}_{bus}$ could be easily calculated. The elements of this matrix include real part $\boldsymbol{G}$ and imaginary part $\boldsymbol{B}$. Since the system frequency is variable in islanded microgrids, these parts, which depend on the frequency, are not considered constant, unlike conventional methods. Considering that balanced networks are studied in this paper, only the positive sequence of impedance and admittance of branches are used.

The branch between bus i and bus k of the system has a series admittance element in the π model that consists of r_{ik} and x_{ik}. In addition, $b_{c,ik}$ denotes the shunt admittances resulting from the capacitance of the line between buses i and k. The elements of the $\overline{\boldsymbol{Y}}_{bus}$

matrix which are associated with these buses are depicted in Fig. 1. The series admittance is:

$$\bar{y}_{ik} = \frac{1}{r_{ik}+jx_{ik}} = g_{ik} + jb_{ik}$$
$$g_{ik} = \frac{r_{ik}}{r_{ik}^2+x_{ik}^2}, b_{ik} = -\frac{x_{ik}}{r_{ik}^2+x_{ik}^2} \quad (6)$$

and the shunt elements (e.g. compensators(are:

$$\bar{y}_{i0} = g_{i0} + jb_{i0}, \qquad \bar{y}_{k0} = g_{k0} + jb_{k0} \quad (7)$$

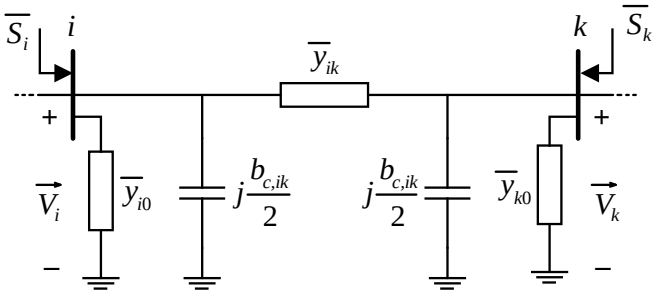

Fig. 1. Effective elements in $\overline{\boldsymbol{Y}}_{bus}$ matrix related to buses i and k.

Based on these parameters, The affected elements of $\overline{\boldsymbol{Y}}_{bus}$ matrix are:

$$\bar{Y}_{ii} = G_{ii} + jB_{ii} = (g_{i0} + \sum_{k\in u} g_{ik}) + j\left(b_{i0} + \sum_{k\in u}\left(b_{ik} + \frac{b_{c,ik}}{2}\right)\right)$$
$$\bar{Y}_{ik} = \bar{Y}_{ki} = G_{ik} + jB_{ik} = -g_{ik} - jb_{ik} \quad (8)$$
$$\bar{Y}_{kk} = G_{kk} + jB_{kk} = (g_{k0} + \sum_{i\in w} g_{ki}) + j\left(b_{k0} + \sum_{i\in w}\left(b_{ki} + \frac{b_{c,ki}}{2}\right)\right)$$

where u and w are the set buses connected to bus i and bus k, respectively.

3. ENR approach for the PF analysis of IMGs

Figure 2 generically represents the i^{th} bus of the modeled microgrid. Based on this figure, the net injected complex power at bus i is

$$\bar{S}_i = P_i + jQ_i = \vec{V}_i\vec{I}_i^* = \vec{V}_i\left(\sum_{j=1}^{N} \bar{Y}_{ij}\vec{V}_j\right)^* \quad (9)$$

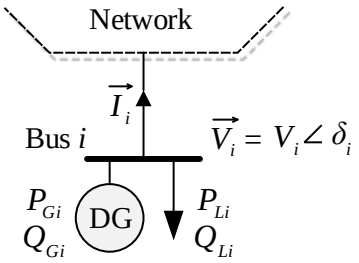

Fig. 2. A generic representation of the bus i of the microgrid.

Hence, PF equations are:

$$P_{Ci} = V_i \sum_{k=1}^{N} V_k [G_{ik} \cos(\delta_i - \delta_k) + B_{ik} \sin(\delta_i - \delta_k)] \quad (10)$$

$$Q_{Ci} = V_i \sum_{k=1}^{N} V_k [G_{ik} \sin(\delta_i - \delta_k) - B_{ik} \cos(\delta_i - \delta_k)] \quad (11)$$

where P_{Ci} and Q_{Ci} are respectively the calculated real and reactive power supplied by bus i. Besides, the scheduled real and reactive power at bus i are:

$$P_i = P_{Gi} - P_{Li} \quad (12)$$

$$Q_i = Q_{Gi} - Q_{Li} \quad (13)$$

The calculated powers (10) and (11) are respectively compared to the scheduled values (12) and (13) to obtain the mismatch matrix, which contains ΔP and ΔQ. The grid-connected operation mode, which uses conventional methods, is based on forming a Jacobian matrix. Since the voltage magnitude of the slack bus is pre-specified and the system frequency is constant, the active and reactive mismatch powers for the slack bus are not considered. Therefore, in the Conventional PF (CPF) method, deal with (14) in which ΔP and ΔQ for the slack bus, as well as ΔP and for PV bus is not considered.

$$\begin{bmatrix} \boldsymbol{\Delta P} \\ \boldsymbol{\Delta Q} \end{bmatrix} = -[\boldsymbol{J}] \begin{bmatrix} \boldsymbol{\Delta \delta} \\ \boldsymbol{\Delta V} \end{bmatrix} \quad (14)$$

where

$$\Delta \bar{S}_i(\boldsymbol{\delta}, \boldsymbol{V}) = \bar{S}_{Ci}(\boldsymbol{\delta}, \boldsymbol{V}) - \bar{S}_i = \bar{S}_{Ci}(\boldsymbol{\delta}, \boldsymbol{V}) + \bar{S}_{Li} - \bar{S}_{Gi} \quad (15)$$

in which $\bar{S}_i$ denotes complex power at bus i. As stated in (15), in CPF methods $\bar{S}_i$ is constant. Therefore, the elements of the Jacobian matrix $\boldsymbol{J}$ are equal to the differentiation of $\bar{S}_{Ci}$ with respect to variables $\boldsymbol{\delta}$ and $\boldsymbol{V}$; in this regard, f is constant. Once the Jacobian matrix is obtained, variables for the $(t+1)$ iteration can be calculated as

$$\begin{bmatrix} \boldsymbol{\delta} \\ \boldsymbol{V} \end{bmatrix}^{(t+1)} = \begin{bmatrix} \boldsymbol{\delta} \\ \boldsymbol{V} \end{bmatrix}^{(t)} - \left[\boldsymbol{J}^{(t)}\right]^{-1} \begin{bmatrix} \boldsymbol{\Delta P} \\ \boldsymbol{\Delta Q} \end{bmatrix}^{(t)} \quad (16)$$

However, in islanded microgrids, the scheduled powers P_i and Q_i are not constant, and they change based on the system's operating point, which depends on droop and load parameters. Moreover, in islanded microgrids, the concept of using a slack bus is invalid. Therefore, two unknown variables, f and V_{RB} (voltage magnitude of the reference bus),

are added to the PF problem, which needs two extra equations. In [5], the active and reactive power equations for the total system losses are considered, while in this work, mismatch equations for the reference bus are considered to cope with this issue.

$$P_{C(RB)} = V_{RB}\sum_{k=1}^{N} V_k\left[G_{(RB)k}\cos(\delta_{RB}-\delta_k) + B_{(RB)k}\sin(\delta_{RB}-\delta_k)\right] \quad (17)$$

$$Q_{C(RB)} = V_{RB}\sum_{k=1}^{N} V_k\left[G_{(RB)k}\sin(\delta_{RB}-\delta_k) - B_{(RB)k}\cos(\delta_{RB}-\delta_k)\right] \quad (18)$$

Therefore, (15) is modified as follows,

$$\Delta\bar{S}_i(f,\boldsymbol{\delta},\boldsymbol{V}) = \bar{S}_{Ci}(f,\boldsymbol{\delta},\boldsymbol{V}) - \bar{S}_i(f,\delta_i,V_i) = \bar{S}_{Ci}(f,\boldsymbol{\delta},\boldsymbol{V}) + \bar{S}_{Li}(f,V_i) - \bar{S}_{Gi}(f,V_i) \quad (19)$$

and the mismatch equations will be

$$\begin{bmatrix}\boldsymbol{\Delta P}\\ \boldsymbol{\Delta Q}\end{bmatrix} = -[\boldsymbol{J}_E]\begin{bmatrix}\Delta f\\ \boldsymbol{\Delta\delta}\\ \boldsymbol{\Delta V}\end{bmatrix} \quad (20)$$

where $\boldsymbol{\Delta P}$ and $\boldsymbol{\Delta Q}$ comprise ΔP_{RB} and ΔQ_{RB}, and $\boldsymbol{\Delta V}$ comprises V_{RB}. Besides, the voltage angle of the reference bus is pre-specified and is not considered in $\boldsymbol{\Delta\delta}$, like the CPF method. Hence, variables for $(t+1)$ iteration can be calculated as

$$\begin{bmatrix}f\\ \boldsymbol{\delta}\\ \boldsymbol{V}\end{bmatrix}^{t+1} = \begin{bmatrix}f\\ \boldsymbol{\delta}\\ \boldsymbol{V}\end{bmatrix}^{t} - \left[\boldsymbol{J}_E{}^{(t)}\right]^{-1}\begin{bmatrix}\boldsymbol{\Delta P}\\ \boldsymbol{\Delta Q}\end{bmatrix}^{t} \quad (21)$$

The enhanced Jacobian matrix $\boldsymbol{J_E}$ contains six sub-matrices as follows,

$$[\boldsymbol{J}_E] = \begin{bmatrix}\boldsymbol{J}_{Pf(N\times1)} & \boldsymbol{J}_{P\delta(N\times(N-1))} & \boldsymbol{J}_{PV(N\times N)}\\ \boldsymbol{J}_{Qf(N\times1)} & \boldsymbol{J}_{Q\delta(N\times(N-1))} & \boldsymbol{J}_{QV(N\times N)}\end{bmatrix} \quad (22)$$

where

$$\begin{aligned}
&\boldsymbol{J}_{Pf} = \begin{bmatrix}\frac{\partial\Delta P_1}{\partial f} & \cdots & \frac{\partial\Delta P_N}{\partial f}\end{bmatrix}^T, \quad \boldsymbol{J}_{Qf} = \begin{bmatrix}\frac{\partial\Delta Q_1}{\partial f} & \cdots & \frac{\partial\Delta Q_N}{\partial f}\end{bmatrix}^T\\
&\boldsymbol{J}_{P\delta} = \begin{bmatrix}\frac{\partial\Delta P_1}{\partial\delta_2} & \cdots & \frac{\partial\Delta P_1}{\partial\delta_N}\\ \vdots & \ddots & \vdots\\ \frac{\partial\Delta P_N}{\partial\delta_2} & \cdots & \frac{\partial\Delta P_N}{\partial\delta_N}\end{bmatrix}, \quad \boldsymbol{J}_{Q\delta} = \begin{bmatrix}\frac{\partial\Delta Q_1}{\partial\delta_2} & \cdots & \frac{\partial\Delta Q_1}{\partial\delta_N}\\ \vdots & \ddots & \vdots\\ \frac{\partial\Delta Q_N}{\partial\delta_2} & \cdots & \frac{\partial\Delta Q_N}{\partial\delta_N}\end{bmatrix}\\
&\boldsymbol{J}_{PV} = \begin{bmatrix}\frac{\partial\Delta P_1}{\partial V_1} & \cdots & \frac{\partial\Delta P_1}{\partial V_N}\\ \vdots & \ddots & \vdots\\ \frac{\partial\Delta P_N}{\partial V_1} & \cdots & \frac{\partial\Delta P_N}{\partial V_N}\end{bmatrix}, \quad \boldsymbol{J}_{QV} = \begin{bmatrix}\frac{\partial\Delta Q_1}{\partial V_1} & \cdots & \frac{\partial\Delta Q_1}{\partial V_N}\\ \vdots & \ddots & \vdots\\ \frac{\partial\Delta Q_N}{\partial V_1} & \cdots & \frac{\partial\Delta Q_N}{\partial V_N}\end{bmatrix}
\end{aligned} \quad (23)$$

where T stands for the transpose operator. It is worth noting that without loss of generality, bus 1 is considered as RB. Moreover, like in the CPF method, the equations

relating $\boldsymbol{\Delta P}$ and voltage magnitude variables for the buses operated in PV mode are not considered.

Detailed expressions of the partial terms in (23) are as follows.

$$\frac{\partial \Delta P_i}{\partial f} = \frac{\partial P_{Ci}}{\partial f} + \frac{\partial P_{Li}}{\partial f} - \frac{\partial P_{Gi}}{\partial f} = \frac{\partial P_{Ci}}{\partial f} + P_{Loi} L_{pfi} \left(\frac{V_i}{V_{oi}}\right)^{L_{pvi}} - G_{pfi} \tag{24}$$

$$\frac{\partial \Delta Q_i}{\partial f} = \frac{\partial Q_{Ci}}{\partial f} + \frac{\partial Q_{Li}}{\partial f} - \frac{\partial Q_{Gi}}{\partial f} = \frac{\partial Q_{Ci}}{\partial f} + Q_{Loi} L_{qfi} \left(\frac{V_i}{V_{oi}}\right)^{L_{qvi}} - G_{qfi} \tag{25}$$

$$\frac{\partial \Delta P_i}{\partial \delta_i} = \frac{\partial P_{Ci}}{\partial \delta_i} \tag{26}$$

$$\frac{\partial \Delta Q_i}{\partial \delta_i} = \frac{\partial Q_{Ci}}{\partial \delta_i} \tag{27}$$

$$\frac{\partial \Delta P_i}{\partial V_i} = \frac{\partial P_{Ci}}{\partial V_i} + \frac{\partial P_{Li}}{\partial V_i} - \frac{\partial P_{Gi}}{\partial V_i} = \frac{\partial P_{Ci}}{\partial V_i} + P_{Loi} \left(1 + L_{pfi}(f - f_o)\right) \left(\frac{L_{pvi}}{V_{oi}}\right) \left(\frac{V_i}{V_{oi}}\right)^{L_{pvi}-1} - G_{pvi} \tag{28}$$

$$\frac{\partial \Delta Q_i}{\partial V_i} = \frac{\partial Q_{Ci}}{\partial V_i} + \frac{\partial Q_{Li}}{\partial V_i} - \frac{\partial Q_{Gi}}{\partial V_i} = \frac{\partial Q_{Ci}}{\partial V_i} + Q_{Loi} \left(1 + L_{qfi}(f - f_o)\right) \left(\frac{L_{qvi}}{V_{oi}}\right) \left(\frac{V_i}{V_{oi}}\right)^{L_{qvi}-1} - G_{qvi} \tag{29}$$

where $\frac{\partial P_{Ci}}{\partial \delta_i}$ and $\frac{\partial Q_{Ci}}{\partial \delta_i}$ in(26) and (27), and the first terms of (28) and (29) (i.e., $\frac{\partial P_{Ci}}{\partial V_i}$ and $\frac{\partial Q_{Ci}}{\partial V_i}$) are similar to the Jacobian matrix of the conventional method. In other words, since P_{Gi}/P_{Li} and Q_{Gi}/Q_{Li} are only related to the voltage magnitude of the corresponding bus (i.e., bus i), the off-diagonal elements of (26) and (27) are similar to the Jacobian of the conventional method. It should be noted that the later terms in (24), (25),)28), and (29) for diagonal elements of the modified Jacobian matrix are not considered in [5]. In this paper, in order to calculate $\frac{\partial P_{Ci}}{\partial f}$ and $\frac{\partial Q_{Ci}}{\partial f}$, (10) and (11) are re-written as,

$$P_{Ci} = V_i^2 G_{ii} + V_i \sum_{k=1,k\neq i}^{N} V_k [G_{ik} \cos(\delta_i - \delta_k) + B_{ik} \sin(\delta_i - \delta_k)] \tag{30}$$

$$Q_{Ci} = -V_i^2 B_{ii} + V_i \sum_{k=1,k\neq i}^{N} V_k [G_{ik} \sin(\delta_i - \delta_k) - B_{ik} \cos(\delta_i - \delta_k)] \tag{31}$$

Therefore, differentiating P_{Ci} and $Q_{Ci}$with respect to f yields,

$$\frac{\partial P_{Ci}}{\partial f} = V_i^2 \frac{\partial G_{ii}}{\partial f} + V_i \sum_{k=1,k\neq i}^{N} V_k \left[\frac{\partial G_{ik}}{\partial f} \cos(\delta_i - \delta_k) + \frac{\partial B_{ik}}{\partial f} \sin(\delta_i - \delta_k)\right] \tag{32}$$

$$\frac{\partial Q_{Ci}}{\partial f} = -V_i^2 \frac{\partial B_{ii}}{\partial f} + V_i \sum_{k=1,k\neq i}^{N} V_k \left[\frac{\partial G_{ik}}{\partial f} \sin(\delta_i - \delta_k) - \frac{\partial B_{ik}}{\partial f} \cos(\delta_i - \delta_k)\right] \tag{33}$$

Knowing that $x_{ik} = l_{ik} f$and $b_{c,ik} = c_{ik} f$ where x, l, b, c and f are all in per unit, the elements affected by the system frequency are identified. To calculate the differentiation

of P_{Ci} and $Q_{Ci}$with respect to the frequency, the differentiation of branch parameters (i.e., r, x, and b) and shunt elements connected to buses (i.e., g_0 and b_0) need to be calculated. Note that

$$\frac{\partial x}{\partial f} = l = \frac{x}{f}$$
$$\frac{\partial b}{\partial f} = c = \frac{b}{f} \tag{34}$$

Hence,

$$\frac{\partial G_{ii}}{\partial f} = \sum_{k\in u} \frac{\partial g_{ik}}{\partial f} = \sum_{k\in u} -\frac{2r_{ik}x_{ik}}{\left(r_{ik}^2+x_{ik}^2\right)^2} \times \frac{x_{ik}}{f} \tag{35}$$

$$\frac{\partial G_{ik}}{\partial f} = -\frac{\partial g_{ik}}{\partial f} = \frac{2r_{ik}x_{ik}}{\left(r_{ik}^2+x_{ik}^2\right)^2} \times \frac{x_{ik}}{f} \tag{36}$$

$$\frac{\partial B_{ii}}{\partial f} = \frac{\partial b_{i0}}{\partial f} + \sum_{k\in u}\left(\frac{\partial b_{ik}}{\partial f} + \frac{1}{2}\frac{\partial b_{c,ik}}{\partial f}\right) = \frac{b_{i0}}{f} + \sum_{k\in u}\left(-\frac{\left(r_{ik}^2+x_{ik}^2\right)-2x_{ik}^2}{\left(r_{ik}^2+x_{ik}^2\right)^2} \times \frac{x_{ik}}{f} + \frac{1}{2}\frac{b_{c,ik}}{f}\right) \tag{37}$$

$$\frac{\partial B_{ik}}{\partial f} = -\frac{\partial b_{ik}}{\partial f} = \frac{\left(r_{ik}^2+x_{ik}^2\right)-2x_{ik}^2}{\left(r_{ik}^2+x_{ik}^2\right)^2} \times \frac{x_{ik}}{f} \tag{38}$$

4. Numerical results

Simulations are conducted in the Matlab environment, in which the MATPOWER package [25] with the proposed ENR solution method is used. For comprehensive analysis, five test systems with different scales (i.e., small, medium and large), different topologies (i.e., radial or meshed), different droop control strategies and different load models are studied. The characteristics of the systems are summerized in Table 1. All simulations are performed using an Intel Core i7-4510U, 2.0-2.6 GHz, RAM 8 GB, personal computer. Note that all the reported amounts in the tables and the figures are in per unit, unless otherwise stated. It is worth noting that, in all test systems and cases, the amounts of P_0 and Q_0 are set zero. The convergence tolerance is set to 10^{-5}. The reported computational times have been obtained as the mean value of 1000 simulations, in order to minimize the influence of other computational activities.

Table 1. Main characteristics of the studied test systems

# System	Name	Scale	# Test Case	Topology

1	The 7-bus	Small	5	Radial
2	The 33-bus	Small	2	Radial/Meshed
3	The 38-bus	Small	2	Radial
4	The 118-bus	Medium	3	Meshed
5	The 1k5-bus	Large	4	Meshed

4.1. Validation and verification of the results

In this section, validation of the proposed ENR approach is provided by comparing the obtained results with the steady-state results of TD simulation done by PLECS software. Furthermore, the reported results of other methods presented in [15], [16], and [21] are compared to verify the obtained results. Further information regarding system modeling in PLECS is available in the Appendix A. Results of the proposed methods are compared with the steady-state values of TD simulations, as well as with the obtained results of Iterative-based methods Utilizing Conventional PF (IUCPF): 3-loop (3L) [16], 2-loop (2L) [15], and 1-loop (1L) [21]. The available results of two modifications of Backward/Forward Sweep (BFS) methods in [6] and [8] are also compared.

(a) The 7-bus test system

A small-scale islanded microgrid, introduced in [15], operating in 0.4 kV line to line voltage and 50 Hz frequency is shown in Fig. 3. Lines and loads information and information of DGs with a base power of 10 kVA are depicted in this figure. Five different cases are considered for this system in which DGs' droop coefficients and their settings for the first four cases are presented in Table A1 in Appendix. The results of these cases are tabulated in Tables 2 to 5. It should be noted that IUCPF versions 2L and 3L can only handle the conventional droop modes of DGs, while the 1L version can handle all droop modes. Hence, in Tables 3 and 4, only the results of IUCPF-1L and the proposed ENR methods have been presented, along with the results conducted by PLECS. The tiny differences observed in the results of the PF analyses compared to the results of PLECS

in some cases are distinguished in **bold**. In addition, the effect of the load model can be easily recognized with the difference in the demanded power of the loads.

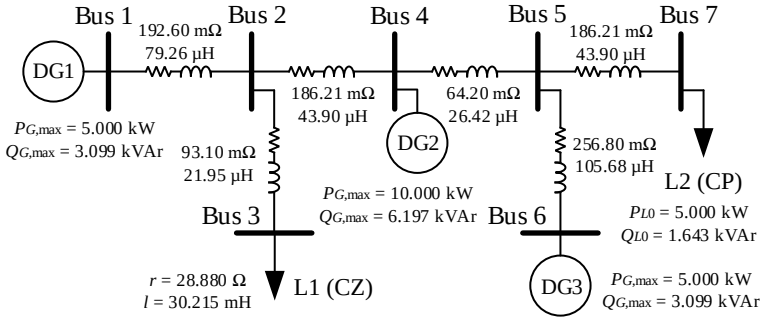

Fig. 3. The 7-bus test system [15].

Table 2. PF results for the 7-bus test system- Case 1

Solution Method		PLECS		IUCPF						Proposed ENR	
				3L [16]		2L [15]		1L [21]			
Frequency (p.u.)		1.00048		1.00048		1.00048		1.00048		1.00048	
Buses Voltage	1	0.9738	0.0000	0.9738	0.0000	0.9738	0.0000	0.9738	0.0000	0.9738	0.0000
	2	0.9706	0.0363	0.9706	0.0363	0.9706	0.0363	0.9706	0.0363	0.9706	0.0363
	3	0.9677	0.0786	0.9677	0.0786	0.9677	0.0786	0.9677	0.0786	0.9677	0.0786
V (p.u.) δ (deg)	4	0.9734	-0.0034	0.9734	-0.0034	0.9734	-0.0034	0.9734	**-0.0033**	0.9734	-0.0034
	5	0.9723	0.0108	0.9723	0.0108	0.9723	0.0108	0.9723	0.0108	0.9723	0.0108
	6	0.9765	-0.0294	0.9765	-0.0294	0.9765	-0.0294	0.9765	**-0.0293**	0.9765	-0.0294
	7	0.9661	0.1011	0.9661	0.1011	0.9661	0.1011	0.9661	0.1011	0.9661	0.1011
Generation	DG1	2.4404	0.8126	2.4404	0.8126	2.4404	0.8126	2.4404	0.8126	2.4404	0.8126
	DG2	4.8807	1.6479	4.8807	1.6479	4.8807	1.6479	4.8807	1.6479	4.8807	1.6479
P_G Q_G	DG3	2.4404	0.7297	2.4404	0.7297	2.4404	0.7297	2.4404	0.7297	2.4404	0.7297
Load	L1	4.6822	1.5397	4.6822	1.5397	4.6822	1.5397	4.6822	1.5397	4.6822	1.5397
P_L Q_L	L2	5.0000	1.6434	5.0000	1.6434	5.0000	1.6434	5.0000	1.6434	5.0000	1.6434
Comp. Time (s)		50		0.2013		0.0754		0.0156		0.0078	

Table 3. PF results for the 7-bus test system- Case 2

Solution Method		PLECS		IUCPF-1L [21]		Proposed ENR	
Frequency (p.u.)		1.00505		1.00505		1.00505	
Buses Voltage	1	0.9520	0.0000	0.9520	0.0000	0.9520	0.0000
	2	0.9488	0.0359	0.9488	0.0359	0.9488	0.0359
	3	0.9460	0.0784	0.9460	0.0784	0.9460	0.0784
V (p.u.) δ (deg)	4	0.9514	-0.0041	0.9514	-0.0041	0.9514	-0.0041
	5	0.9502	0.0088	0.9502	0.0088	0.9502	0.0088
	6	0.9542	-0.0404	0.9542	-0.0404	0.9542	-0.0404
	7	0.9439	0.1033	0.9439	0.1033	0.9439	0.1033
Generation	DG1	2.4023	0.7818	2.4023	0.7818	2.4023	0.7818
	DG2	4.8583	1.5636	**4.8582**	1.5636	4.8583	1.5636
P_G Q_G	DG3	2.2887	0.7818	2.2887	0.7818	2.2887	0.7818
Load	L1	4.4699	1.4766	4.4699	1.4766	4.4699	1.4766
P_L Q_L	L2	5.0000	1.6434	5.0000	1.6434	5.0000	1.6434
Comp. Time (s)		30		0.0880		0.0138	

Table 4. PF results for the 7-bus test system- Case 3

Solution Method			PLECS		IUCPF-1L [21]		Proposed ENR	
Frequency (p.u.)			0.99365		0.99365		0.99365	
Buses Voltage		1	0.9373	0.0000	0.9373	0.0000	0.9373	0.0000
		2	0.9341	0.0371	0.9341	0.0371	0.9341	**0.0370**
		3	0.9313	0.0792	0.9313	0.0792	0.9313	**0.0791**
V (p.u.)	δ (deg)	4	0.9367	-0.0010	0.9367	-0.0010	0.9367	-0.0010
		5	0.9355	0.0142	0.9355	0.0142	**0.9354**	0.0142
		6	0.9395	-0.0299	0.9395	-0.0299	0.9395	-0.0299
		7	0.9290	0.1120	0.9290	0.1120	0.9290	0.1120
Generation		DG1	2.3622	0.7737	2.3622	**0.7738**	2.3622	0.7737
		DG2	4.7547	1.5778	**4.7546**	1.5778	4.7547	1.5778
P_G	Q_G	DG3	2.3056	0.7172	2.3056	0.7172	**2.3057**	0.7172
Load		L1	4.3424	1.4182	4.3424	1.4182	4.3424	1.4182
P_L	Q_L	L2	5.0000	1.6434	5.0000	1.6434	5.0000	1.6434
Comp. Time (s)			20		0.0380		0.0123	

Table 5. PF results for the 7-bus test system- Case 4

Solution Method			PLECS		IUCPF-1L [21]		Proposed ENR	
Frequency (p.u.)			0.99203		0.99203		0.99203	
Buses Voltage		1	0.9924	0.0000	0.9924	0.0000	0.9924	0.0000
		2	0.9900	-0.0015	0.9900	-0.0015	0.9900	-0.0015
		3	0.9871	0.0405	**0.9870**	0.0405	**0.9870**	0.0405
V (p.u.)	δ (deg)	4	0.9935	-0.0791	0.9935	-0.0791	0.9935	-0.0791
		5	0.9932	-0.1046	**0.9931**	-0.1046	**0.9931**	-0.1046
		6	1.0000	-0.2539	1.0000	-0.2539	1.0000	-0.2539
		7	0.9872	-0.0507	0.9872	-0.0507	0.9872	-0.0507
Generation		DG1	1.9923	0.2342	1.9923	0.2342	1.9923	0.2342
		DG2	3.9846	0.4012	3.9846	0.4012	3.9846	0.4012
P_G	Q_G	DG3	4.0000	2.1249	4.0000	2.1249	4.0000	2.1249
Load		L1	4.8789	1.5908	4.8789	1.5908	4.8789	1.5908
P_L	Q_L	L2	5.0000	1.6434	5.0000	1.6434	5.0000	1.6434
Comp. Time (s)			20		0.05644		0.0109	

In Case 1, it is assumed that all DGs are operating in the conventional droop mode. In Case 2, it is supposed that the output impedance of DGs is resistive and all the DGs operate in the inversed droop mode, while in Case 3, it is assumed that all the DGs operate in the complex mode. In Case 4, the mixed operation of DGs droop modes is considered. The operating modes of DG1 and DG2 are conventional, and DG3 operates in PV mode. In addition, in this case, for evaluating the efficiency of the proposed formulation in the presence of a parallel compensator, a capacitor with the capacity of 500 var at nominal voltage and frequency is placed at bus 7.

In order to statistically assess the performance of the proposed method, a Monte-Carlo simulations is performed to extract true statistical conclusions on the validation of the

proposed method's performance. Therefore, in Case 5, for each of the system loads 10 values are randomly selected in the range of [0.5 to 1.5] times of the nominal load (indicating light-load to heavy-load conditions), which is presented in Table 6. These values are sequentially applied to the loads and as a result are the injected power of DGs in the time domain extracted by PLECS are shown in Fig. 4. Besides, for more accurate analysis and validation of the results of the proposed method, the PF results for the third and seventh intervals are compared with the steady-state results of PLECS in Table 7. It should be noted that the droop mode in this case is similar to the first case (i.e., inductive). Therefore, as can be seen from Fig. 4 and Table 7, due to the globality of the frequency quantity and the relationship of real power to it in this type of control mode (based on (1)) the active power sharing is precisely done, while for reactive power it is not.

Table 6. Load factors (LF) for the Case 5 of the 7-bus test system

# Interval	1	2	3	4	5	6	7	8	9	10
LF for Load 1	1.3	1.4	0.6	1.1	0.8	1.0	1.5	0.7	0.9	1.2
LF for Load 2	0.8	1.2	0.7	0.6	1.0	1.5	1.1	1.3	1.4	0.9

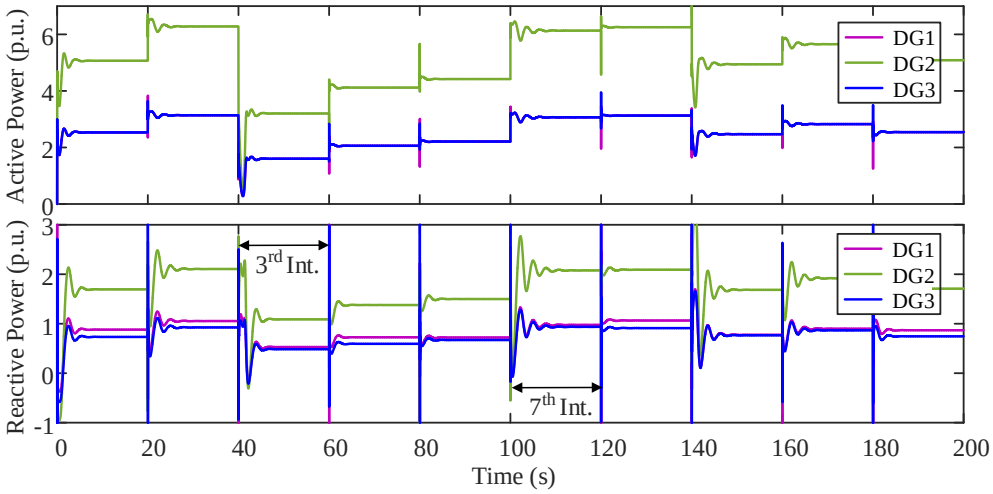

Fig. 4. Injected active and reactive power of DGs in the 7-bus test system for the Case 5.

Table 7. PF results for the 7-bus test system- Case 5

# Time Interval		3				7			
Solution Method		PLECS		ENR		PLECS		ENR	
Frequency (p.u.)		1.0072		1.0072		0.9950		0.9950	
Buses Voltage	1	0.9829	0.0000	0.9829	0.0000	0.9656	0.0000	0.9656	0.0000
	2	0.9809	0.0229	0.9809	0.0229	0.9615	0.0493	0.9615	0.0493
	3	0.9791	0.0485	0.9791	0.0485	0.9573	0.1124	0.9573	0.1124
V (p.u.) δ (deg)	4	0.9824	0.0003	0.9824	0.0003	0.9663	-0.0160	0.9663	-0.0160
	5	0.9816	0.0103	0.9816	0.0103	0.9652	-0.0015	0.9652	-0.0015
	6	0.9843	-0.0161	0.9843	-0.0161	0.9706	-0.0515	0.9706	-0.0515
	7	0.9773	0.0721	0.9773	0.0721	0.9584	0.0996	0.9584	0.0996
Generation	DG1	1.6016	0.5293	1.6015	0.5293	3.1275	1.0654	3.1275	1.0654
	DG2	3.2031	1.0891	3.2031	1.0891	6.2551	2.0914	6.2551	2.0914
P_G Q_G	DG3	1.6016	0.4858	1.6016	0.4858	3.1275	0.9123	3.1275	0.9123
Load	L1	2.8720	0.9508	2.8720	0.9508	6.8794	2.2498	6.8794	2.2498
P_L Q_L	L2	3.5000	1.1504	3.5000	1.1504	5.5000	1.8077	5.5000	1.8077

(b) The 33-bus test system

The well-known Baran & Wu 33-bus distribution network [26] is adoptod to construct an islanded microgrid [6], [8]. The nominal frequency and voltage of the system is 60 Hz and 12.66 kV, respectively. Data about the line impedances and system loads can be found in [26]. Five DGs, as shown in Fig. 5, are added to the orginally passive network to supply the loads in islanded operation. Two test cases with the inductive droop mode of DGs with the characteristics presented in [8] and in the Table A2 in the Appendix are considered. In addition, to have a compatible comparison with the previous study on this system, all loads are modeled as constant power. The radial system (with the black branches in Fig. 5) is considered in the first case. The performance efficiency of the proposed method in the face of meshed network is evaluated in the latter case. This system have five normally open looping branches, which two of them (as drown in blue colour in Fig. 5) are closed to make the weakly meshed system. Similar to [8], the base power is considered 0.5 MVA, and the set-point for system frequency, f_0, and voltage of all DGs, V_0, is set to 1 p.u. The PF results for the 33-bus test system are presented in Table 8. Due to the space limitations, the buses voltage angles and injected power by DGs are not reported here.

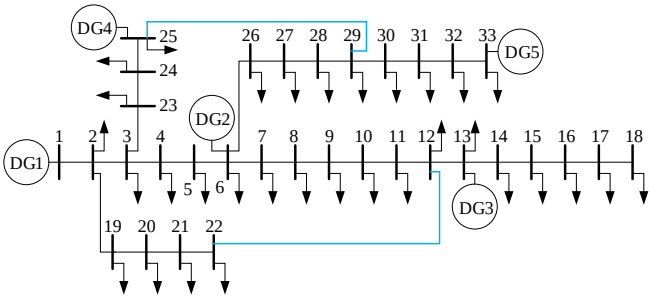

Fig. 5. The 33-bus test system [8].

Table 8. PF results for the 33-bus test system- frequency, buses voltage magnitude, and computational time

Test Case		Case 1				Case 2			
Solution Method		PLECS	DBFS [6]	MBFS [8]	ENR	PLECS	IUCPF		ENR
							3L [16]	1L [21]	
Frequency (p.u.)		0.9984	0.9984	0.9984	0.9984	0.9984	0.9984	0.9984	0.9984
Buses Voltage Magnitude	1	0.9882	**0.9858**	0.9882	0.9882	0.9875	0.9875	0.9875	0.9875
	2	0.9874	**0.9849**	0.9874	0.9874	0.9867	0.9867	0.9867	0.9867
	3	0.9848	**0.9820**	0.9848	0.9848	0.9839	0.9839	0.9839	0.9839
	4	0.9838	**0.9807**	0.9838	0.9838	0.9832	0.9832	0.9832	0.9832
	5	0.9832	**0.9798**	0.9832	0.9832	0.9829	0.9829	0.9829	0.9829
	6	0.9812	**0.9768**	0.9812	0.9812	0.9822	0.9822	0.9822	0.9822
	7	0.9795	**0.9750**	0.9795	0.9795	0.9809	0.9809	0.9809	0.9809
	8	0.9788	**0.9743**	0.9788	0.9788	0.9798	0.9798	0.9798	0.9798
	9	0.9789	**0.9743**	0.9789	0.9789	0.9797	0.9797	0.9797	0.9797
	10	0.9795	**0.9748**	0.9795	0.9795	0.9802	0.9802	0.9802	0.9802
	11	0.9798	**0.9750**	0.9798	0.9798	0.9803	0.9803	0.9803	0.9803
	12	0.9804	**0.9756**	0.9804	0.9804	0.9808	0.9808	0.9808	0.9808
	13	0.9834	**0.9784**	0.9834	0.9834	0.9837	0.9837	0.9837	0.9837
	14	0.9813	**0.9763**	0.9813	0.9813	0.9816	0.9816	0.9816	0.9816
	15	0.9799	**0.9750**	0.9799	0.9799	0.9802	0.9802	0.9802	0.9802
	16	0.9787	**0.9737**	0.9787	0.9787	0.9790	0.9790	0.9790	0.9790
	17	0.9768	**0.9718**	0.9768	0.9768	0.9771	0.9771	0.9771	0.9771
	18	0.9762	**0.9712**	0.9762	0.9762	0.9765	0.9765	0.9765	0.9765
	19	0.9868	**0.9844**	0.9868	0.9868	0.9862	0.9862	0.9862	0.9862
	20	0.9832	**0.9808**	0.9832	0.9832	0.9826	0.9826	0.9826	0.9826
	21	0.9825	**0.9800**	0.9825	0.9825	0.9818	0.9818	0.9818	0.9818
	22	0.9819	**0.9794**	0.9819	0.9819	0.9809	0.9809	0.9809	0.9809
	23	0.9839	**0.9810**	**0.9838**	0.9839	0.9822	0.9822	0.9822	0.9822
	24	0.9825	**0.9796**	0.9825	0.9825	0.9792	0.9792	0.9792	0.9792
	25	0.9845	**0.9815**	0.9845	0.9845	0.9796	0.9796	0.9796	0.9796
	26	0.9805	**0.9760**	0.9805	0.9805	0.9818	0.9818	0.9818	0.9818
	27	0.9796	**0.9750**	0.9796	0.9796	0.9812	0.9812	0.9812	0.9812
	28	0.9762	**0.9706**	0.9762	0.9762	0.9794	0.9794	0.9794	0.9794
	29	0.9739	**0.9676**	0.9739	0.9739	0.9785	0.9785	0.9785	0.9785
	30	0.9733	**0.9668**	0.9733	0.9733	0.9777	0.9777	0.9777	0.9777
	31	0.9766	**0.9691**	0.9766	0.9766	0.9803	0.9803	0.9803	0.9803
	32	0.9782	**0.9704**	0.9782	0.9782	0.9817	0.9817	0.9817	0.9817
	33	0.9812	**0.9729**	0.9812	0.9812	0.9843	0.9843	0.9843	0.9843
Comp. Time (s)		25	-	-	0.0075	25	0.5120	0.2173	0.0079

One of the effective, robust and widely used methods for PF analysis in distribution systems (which is applicable for radial and meshed network) is Backward/Forward Sweep (BFS) approach [28]. Two adaptation of this approach for PF analysis of islanded microgrid proposed in [6] and [8] which are named Direct Backward/Forward Sweep (DBFS) and Modified Backward/Forward Sweep (MBFS), repectively. The reults of these methods are only available for the Case 1. Besides, the results of our proposed ENR methods as well as the PLECS results are also shown in this case. Unlike DBFS method, which inherently uses approximation [6], the results of the other methods are consistent. It should be noted that due to the fact that the implementation of BFS methods is outside the scope of this work, the reported computational time in [8] is not mentioned in Table 8 due to differences in the hardware used. However, the computational time in BFS methods is basically longer compared to NR method due to the nature of the methods, which indicates the superiority of our ENR method in computational speed.

Referring to Table 8, the correspondences of the PF results of ENR and IUCPF methods with the PLECS results are observed, which shows the efficiency of the PF analysis methods in terms of mesh systems, too.

(c) The 38-bus test system

The single line diagram of the 38-bus test system orginated from the 33-bus distribution network is shown in Fig. 6 [5]. Reffering to this figure, five buses have been added in this system to connect the DGs through the transformer to the network [5]. Different frequency and voltage dependencies for the loads at different buses have been utilized based on classifying the loads as residential (R), commercial (C), or industrial (I), as established in Table 9 [27]. Similar to [5], the base power is considered 1 MVA, and the set-point for frequency, f_0, is set to 1 p.u.. Two cases have been studied. In Case 1, the voltage set-points, V_{0i}, are considered as 1.01 p.u. as in [5] for all DG units, while

these settings are considered 1.03 p.u. in Case 2. The DGs droop coefficients, and DG limitations, are tabulated in Table A3 in the Appendix. The conventional droop mode for DGs is considered here. To further evaluate the performance of the proposed formulation in the presence of lines capacitance, in Case 2, it is assumed that lines with r/x ratio larger than 1.5 have a capacitor with the capacity of 1.6×10^{-6} times their inductance, in Farad.

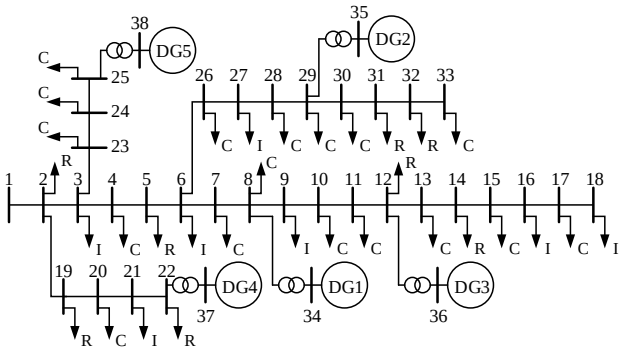

Fig. 6. The 38-bus test system [5].

Table 9. Frequency and voltage-dependent characteristics of loads in the 38-bus test system [27].

Types of load	L_{pf}	L_{pv}	L_{qf}	L_{qv}
Residential (R)	1	0.92	-1	4.04
Industrial (I)	1	0.18	-1	6.00
Commercial (I)	1	1.51	-1	3.40

The system frequency and voltage magnitude of buses in both cases are presented in Table 10. Due to space limitations, the buses' voltage angles are not reported. Moreover, the active and reactive powers of the DGs are tabulated in Table 11. As it can be seen from this table, Q_G of DG5 (at bus 38) exceeds the limit. Hence it has been set to its maximum value.

It is worth noting that the method does not converge for this system as well as the 33-bus test system. Althouth IUCPF (3L) has been proposed as a complement to IUCPF (2L) method to improve its performance in large-scale systems, however it needs some parameter tuning (as mentioned in [16]). A similar issue is observed in IUCPF (1L) method, which is computationally superior to IUCPF (3L). In the three systems studied so far, the accuracy of the proposed ENR method for the different operational cases has

been validated compared to the results of PLECS and verified in comparison with other PF analysis methods. On the other hand, TD simulation for medium-scale and large-scale systems is not logical. Therefore, only the results of the proposed ENR are presented for the following systems, which indicates the solving capability of these systems and the proposed method outperforms other PF analysis methods.

Table 10. PF results for the 38-bus test system- frequency, buses voltage magnitude, and computational time

Test Case		Case 1				Case 2			
Solution Method		PLECS	IUCPF		ENR	PLECS	IUCPF		ENR
			3L [16]	1L [21]			3L [16]	1L [21]	
Frequency (p.u.)		0.99813	0.99813	0.99813	0.99813	0.99444	0.99444	0.99444	0.99444
Buses Voltage Magnitude	1	0.9802	0.9802	0.9802	0.9802	0.9713	0.9713	0.9713	0.9713
	2	0.9802	0.9802	0.9802	0.9802	0.9713	0.9713	0.9713	0.9713
	3	0.9790	0.9790	0.9790	0.9790	0.9710	0.9710	0.9710	0.9710
	4	0.9787	0.9787	0.9787	0.9787	0.9720	0.9720	0.9720	0.9720
	5	0.9787	0.9787	0.9787	0.9787	0.9733	0.9733	0.9733	0.9733
	6	0.9795	0.9795	0.9795	0.9795	0.9768	0.9768	0.9768	0.9768
	7	0.9825	0.9825	0.9825	0.9825	0.9795	0.9795	0.9795	0.9795
	8	0.9834	0.9834	0.9834	0.9834	0.9838	0.9838	0.9838	0.9838
	9	0.9834	0.9834	0.9834	0.9834	0.9854	0.9854	0.9854	0.9854
	10	0.9838	0.9838	0.9838	0.9838	0.9876	0.9876	0.9876	0.9876
	11	0.9838	0.9838	0.9838	0.9838	0.9880	0.9880	0.9880	0.9880
	12	0.9839	0.9839	0.9839	0.9839	0.9888	0.9888	0.9888	0.9888
	13	0.9784	0.9784	0.9784	0.9784	0.9834	0.9834	0.9834	0.9834
	14	0.9764	0.9764	0.9764	0.9764	0.9813	0.9813	0.9813	0.9813
	15	0.9751	0.9751	0.9751	0.9751	0.9801	0.9801	0.9801	0.9801
	16	0.9739	0.9739	0.9739	0.9739	0.9788	0.9788	0.9788	0.9788
	17	0.9721	0.9721	0.9721	0.9721	0.9771	0.9771	0.9771	0.9771
	18	0.9715	0.9715	0.9715	0.9715	0.9765	0.9765	0.9765	0.9765
	19	0.9808	0.9808	0.9808	0.9808	0.9716	0.9716	0.9716	0.9716
	20	0.9872	0.9872	0.9872	0.9872	0.9754	0.9754	0.9754	0.9754
	21	0.9894	0.9894	0.9894	0.9894	0.9769	0.9769	0.9769	0.9769
	22	0.9939	0.9939	0.9939	0.9939	0.9802	0.9802	0.9802	0.9802
	23	0.9785	0.9785	0.9785	0.9785	0.9697	0.9697	0.9697	0.9697
	24	0.9783	0.9783	0.9783	0.9783	0.9677	0.9677	0.9677	0.9677
	25	0.9812	0.9812	0.9812	0.9812	0.9689	0.9689	0.9689	0.9689
	26	0.9796	0.9796	0.9796	0.9796	0.9767	0.9767	0.9767	0.9767
	27	0.9798	0.9798	0.9798	0.9798	0.9767	0.9767	0.9767	0.9767
	28	0.9796	0.9796	0.9796	0.9796	0.9759	0.9759	0.9759	0.9759
	29	0.9799	0.9799	0.9799	0.9799	0.9758	0.9758	0.9758	0.9758
	30	0.9767	0.9767	0.9767	0.9767	0.9726	0.9726	0.9726	0.9726
	31	0.9730	0.9730	0.9730	0.9730	0.9689	0.9689	0.9689	0.9689
	32	0.9722	0.9722	0.9722	0.9722	0.9681	0.9681	0.9681	0.9681
	33	0.9719	0.9719	0.9719	0.9719	0.9679	0.9679	0.9679	0.9679
	34	0.9965	0.9965	0.9965	0.9965	1.0004	1.0004	1.0004	1.0004
	35	0.9993	0.9993	0.9993	0.9993	0.9939	0.9939	0.9939	0.9939
	36	0.9971	0.9971	0.9971	0.9971	1.0045	1.0045	1.0045	1.0045
	37	0.9973	0.9973	0.9973	0.9973	0.9828	0.9828	0.9828	0.9828
	38	0.9848	0.9848	0.9848	0.9848	0.9715	0.9715	0.9715	0.9715
Comp. Time (s)		600	1.4660	0.2510	0.0166	800	0.8192	0.3434	0.0332

Table 11. PF results for the 38-bus test system- active and reactive powers of the DG units: PLECS, IUCPF methods (3L and 1L), and proposed ENR method

Test Case			Case 1		Case 2	
P_G	Q_G	DG1	0.3670	0.6774	0.8075	0.5323
		DG2	1.2467	0.3198	1.0150	0.4333
		DG3	0.4156	0.6442	0.8075	0.4584
		DG4	0.8311	0.2537	0.5075	0.2835
		DG5	0.8311	0.3000	0.5075	0.3000

(d) The 118-bus test system

In the fourth test case, six DG units have benn added to a 11 kV distribution system presented in [25] and [29] to provide the islanded operation of the network depicted in Fig. 7. The main system, which is operated radially, has 15 tie swithes. In this study, five of them (drown in blue in Fig. 7) are considered closed to provide a weakly meshed network. Data about the line impedances and system loads can be found in [25] and [29[, While DGs information is provided in Table A4 of the Appendix B. Three different cases is considered in which the droop control modes are inductive, resistive and complex, respectively. The base power is considered 10 MVA, and the system frequency and voltage set-points for all DGs are set to 1 p.u. and 1.03 p.u., respectively.

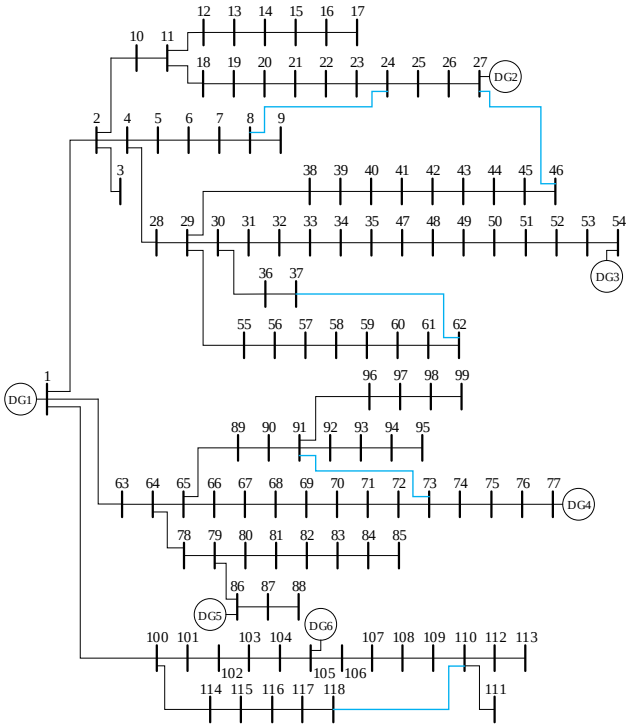

Fig. 7. The modified 118-bus distribution system as an islanded microgrid.

The results of PF analysis using proposed ENR method are presented in Table 12. In addition, the voltage profiles for the three tested cases are shown in Fig. 8.

Table 12. PF results of the proposed ENR method for the 118-bus test system- Active and reactive power of DGs, system frequency and voltage magnitude of DG buses and computational time

Test Cases	Case 1			Case 2			Case 3		
Frequency	0.98944			1.01270			0.99731		
# DG	P_G	Q_G	V	P_G	Q_G	V	P_G	Q_G	V
DG1	0.6326	0.5706	0.9737	0.7700	0.4720	0.9446	0.7070	0.5459	0.9085
DG2	0.3173	0.2263	0.9961	0.2969	0.2360	0.9803	0.3070	0.2262	1.0243
DG3	0.3173	0.1881	0.9914	0.2587	0.2360	0.9642	0.2860	0.2051	0.9296
DG4	0.3173	0.1936	0.9921	0.2704	0.2360	0.9673	0.2905	0.2097	0.9506
DG5	0.3173	0.2324	0.9904	0.3033	0.2360	0.9666	0.3114	0.2306	0.9865
DG6	0.4226	0.3213	0.9927	0.4214	0.3151	0.9678	0.4232	0.3155	0.9415
Comp. Time (s)	0.0164			0.0142			0.0112		

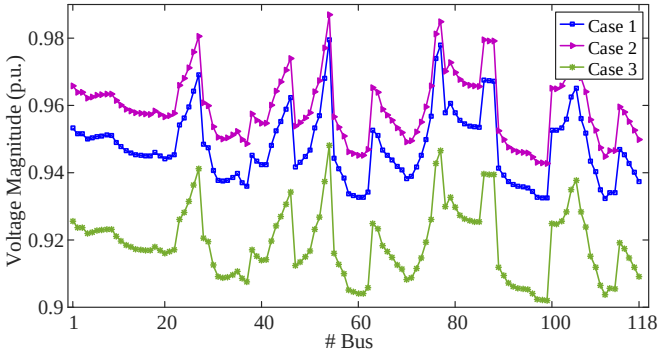

Fig. 8. Voltage profiles of the 118-bus test system for different test cases.

(e) The 1k5-bus test system

The large weakly meshed microgrid with 1458 buses (named 1k5-bus system) introduced in [20]. All system information, including demanded power of loads, line impedances, capacitor banks, and droop coefficients of DGs, is provided in the reference therein [20]. In [20] all loads are modeled as constant power and all DGs operate in inductive droop mode with the coefficients presented in Table A5 in Appendix. In addition, the system frequency and voltage set-points for all DGs are set to 1 p.u.. In this situation, which is analysied as Case 1, the system frequency is less than the permissible limit of 0.98, as defined in Standared EN50160 [30] (see Table 13). For further evalution, considering the base power of 50 MVA, four additional test cases with different droop

modes and coefficients are considered here. In Case 2-Case 4 with the same set-points as Case 1 the droop modes are inductive, resistive and complex, respectively. To observe the effect of voltage set-point, V_{0i}, on the PF results and network parameters, this value is set to 1.05 for all DG units. Reffering to Table 13, it can be seen that the minimum voltage magnitude has increased to 0.9015 p.u.. Another point that can be understood from this table, as we expected, in the case of inductive droop control mode (i.e., Case 1, Case 2 and Case 5), the injected active powers of the DGs with the same capacities and coefficients are equal. These conditions are in the resistive (inverse) droop mode (i.e., Case 3) for the injected reactive powers. Further explanations on this issue are addressed in the subsequent Sub-section. The voltage profiles of buses 600-700 of the syetem, for all tested cases are shown in Fig. 9.

Table 13. PF results of the proposed ENR method for the 1k5-bus test system- Active and reactive power of DGs, system frequency, minimum voltages and computational time.

Test Cases	Case 1		Case 2		Case 3		Case 4		Case 5	
Frequency	0.97657		0.98959		1.00786		0.99419		0.98960	
# DG	P_G	Q_G	P_G	Q_G	P_G	Q_G	P_G	Q_G	P_G	Q_G
DG1	0.4685	0.5253	0.7283	0.4805	1.2809	0.3402	0.8770	0.4710	0.7271	0.4508
DG2	0.4685	0.0785	0.4166	0.0979	0.0000	0.1950	0.3293	0.0971	0.4159	0.0934
DG3	0.4685	0.1714	0.4166	0.1776	0.5632	0.1950	0.4182	0.1860	0.4159	0.1672
DG4	0.4685	0.1575	0.4166	0.1621	0.3952	0.1950	0.3999	0.1677	0.4159	0.1554
DG5	0.4685	0.1919	0.4166	0.1657	0.1076	0.1950	0.3896	0.1574	0.4159	0.1569
DG6	0.4685	0.1467	0.4166	0.1594	0.4679	0.1950	0.3986	0.1664	0.4159	0.1524
$V_{\min}$	Bus 789	0.8749	Bus 846	0.8383	Bus 789	0.7935	Bus 789	0.7879	Bus 789	0.9015
Comp. Time (s)	0.2279		0.2818		0.6646		0.2827		0.2919	

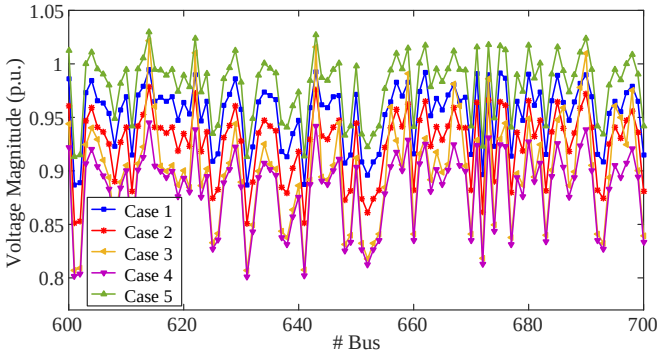

Fig. 9. Voltage profile of the 1k5-bus test system for different test cases- buses 600 to 700.

4.2. Optimal droop-control mode selection through the PSEI analysis

As mentioned before, (Sub-section 2.1) different types of droop-control mode are distinguished depending on the output impedance of the DGs, which depends on the network parameters (branch impedances and the output filter of the DGs). There is no specific method for selecting the type of DG's droop in previous studies. In this paper, an index is introduced which shows the amount of the Power Sharing Error (PSE) as follows. According to the philosophy of the droop-control, it is desirable for the DGs with the same droop coefficients m/n injecting the same amount of output powers of P_G/Q_G So,

$$PSEI = \sum_{i=1}^{N_{DDG}} \left[\left(P_{Gi} - P_{Gi,\mathrm{des}}\right)^2 + \left(Q_{Gi} - Q_{Gi,\mathrm{des}}\right)^2 \right] \quad (39)$$

where $P_{Gi,\mathrm{des}}$ and $Q_{Gi,\mathrm{des}}$ are the desired active and reactive injected powers of DGs, respectively, and N_{DDG} represents the number of droop-controlled DG (DDG) units. The active and reactive power of one of the DDGs is considered as a reference for the desired values, and the desired values of the other DDGs are calculated based on the value of their droop coefficients. With respect to the values of P_G and Q_G presented in the above tables, the $PSEI$ can be calculated as presented in Table 14. The smaller value of *PSEI* in the case of inductive droop in the small 7-bus system, the medium-scale 118-bus and the large-scale 1k5-bus systems compared to resistive or complex modes confirms the designation of inductive droop as the conventional droop control mode in most islanded microgrids [5]. Referring to the Table 14, the effect of the secondary control (i.e., adjustment of set-points) in the 1k5-bus test system on reducing the value of power sharing error is visible (compare the *PSEI* in Case 5 with Case 1). Of course, this issue needs further investigation, which is outside the scope of this work.

4.3. Convergence characteristic of the proposed ENR method in islanded microgrids

The process of changing the normalized mismatches values obtained from (20) in each iteration gives us an overview of the convergence property of the proposed Newton-based methods [31]. Accordingly, to further evaluate the computational efficiency of the

proposed method, the convergence characteristics of all systems in different cases are plotted in Fig. 10. In this figure $\|\boldsymbol{F}(\boldsymbol{x})\|_{\infty}$ means infinit norm of power mismatches (i.e., $\boldsymbol{F}(\boldsymbol{x}) = [\boldsymbol{\Delta P}, \boldsymbol{\Delta Q}\,]^{T}$). As known, NR method has local convergence, and its quadratic properties are only achieved close to the solution. Considering this, the preservation of such a feature in its enhanced version in this paper (i.e., ENR) is also evident, especially in the 33-bus, 118-bus and 1k5-bus systems.

Table 14. The value of PSEI for different droop mode control of DGs

# Sys.	Name	Test Case	Droop Mode	*PSEI* (p.u.)
1	7-bus	Case 1	**Inductive**	7.393×10^{-5}
		Case 2	Resistive	1.578×10^{-4}
		Case 3	Complex	8.233×10^{-5}
		Case 4	Ind. + PV	4.504×10^{-5}
		Case 5 (avg)	Inductive	1.658×10^{-4}
2	33-bus	Case 1	Inductive	0.2516
		Case 2	Inductive	0.0883
3	38-bus	Case 1	Inductive	0.0098
		Case 2	Inductive	0.0379
4	118-bus	Case 1	**Inductive**	0.0277
		Case 2	Resistive	0.0518
		Case 3	Complex	0.0302
5	1k5-bus	Case 1	Inductive	0.7146
		Case 2	**Inductive**	0.0785
		Case 3	Resistive	1.1399
		Case 4	Complex	0.2516
		Case 5	Inductive	0.0669

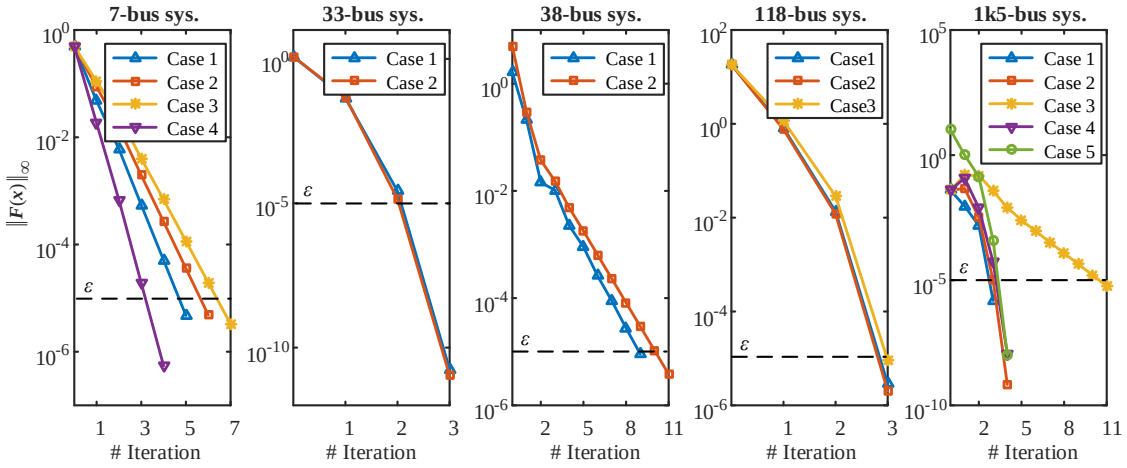

Fig. 10. Convergence characteristics of the test systems

5. Conclusions

In this paper, a novel PF analysis method is proposed for islanded microgrids. The method is based on the well-known NR scheme and tries to enhance it to overcome the limitation of using the scheme in droop-controlled islanded microgrids with variable frequency and without a slack bus. In the presented PF analysis method, any type of droop control scheme can be utilized. Moreover, a complete model of lines, including shunt capacitors, is modeled. Also, different load demand models like constant power, constant current, constant impedance, and also the exponential model are applicable. Shunt elements like power factor correction capacitors are also considered in the modeling. Because of using this comprehensive model, which is based on the NR method, the utilization of this method in the currently available power system analysis tools is highly recommended. Accurate results (as the TD simulation results show) and proper convergence time (compared with different methods previously presented) strengthen this recommendation.

Appendix A. Proposed model of islanded microgrid for TD simulation

In order to validate the proposed PF method in different cases, a TD simulation should be performed for each case. Several computer programs are generally used for that purpose, e.g., Matlab Simulink, PSCAD, PLECS, etc. In this study, PLECS has been used because of its simplicity and higher speed compared with the others. Simulation speed is one of the most important parameters in choosing the appropriate software since a great number of elements (e.g., line impedances, loads, and DGs) are used in these test cases, and it can worsen the problem. For increasing the speed and accuracy of the simulations, several simplifications have been adopted, which will be discussed in the following.

Since the TD simulations are used for validating the proposed PF method, there is no need to simulate the inverter and the filtering stage. As shown in Fig. A1, instead of the

DC link, inverter, filtering stage, and the controllers, three ideal voltage sources are used that can intensively reduce the complexity of the circuit and increase the speed and accuracy. If an inverter and a filter are used instead, the controllers should be tuned in a way that the output voltage follows the reference value generated by the droop stage. Even if that is achieved, it takes much effort, and finally, it will work as an ideal voltage source. Moreover, the speed of the voltage controller should be much higher than that of the droop controller. Therefore, using an ideal voltage source instead of an inverter does not make any difference in the system's dynamic response.

The three ideal voltage sources are directly connected to the grid. Their output voltages and currents are measured to calculate the output active and reactive power and use them in the droop controller. Before the filtered P and Q enter the droop controller, the "Limit" block limits the output power of the DG. When the output Q exceeds the maximum permissible amount ($Q_{G,\max}$), the "Limit" block increases its output gradually so that the droop controller decreases the voltage magnitude (in conventional droop), and therefore less reactive power is injected. Yet, when the reactive power is in the permissible range (from $Q_{G,\min}$ to $Q_{G,\max}$), the actual amount of Q_G is delivered to the droop controller. The same procedure is employed for limiting the active power and also for different droop types.

For simulating different load types (i.e., constant power, constant impedance, residential, industrial, etc.), a set of three-phase currents should be drawn from the grid so that the active and reactive power match the reference values. The procedure for creating these currents is shown in Fig. A2. The first step is measuring the load terminal voltage and calculating the amplitude, frequency, and phase of the voltage.

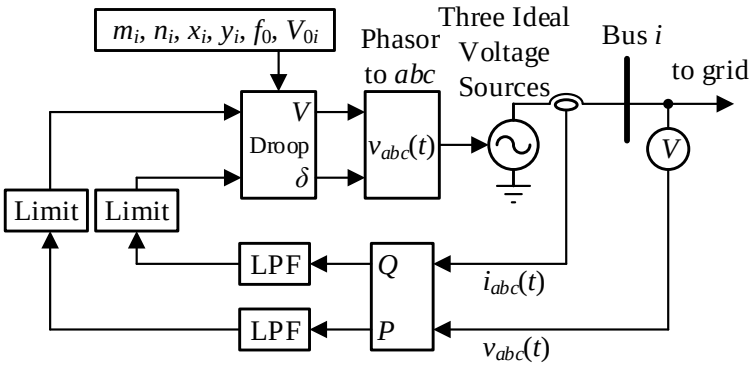

Fig. A1. DG model in TD simulation.

Two Low Pass Filters (LPFs) are then used to decrease the dynamic speed of the load, which helps to make the system more stable. Since the dynamic response of the loads is not the subject of this paper, the cutoff frequencies of these filters can be tuned so that the system reaches the steady-state condition in the shortest time. The outputs of LPFs are used to calculate the active and reactive power of the load (according to (4) and (5)). The needed current can be precisely calculated with the active and reactive power, voltage phase, and voltage amplitude. Then the calculated current is used as the input of an ideal current source to be connected to the grid.

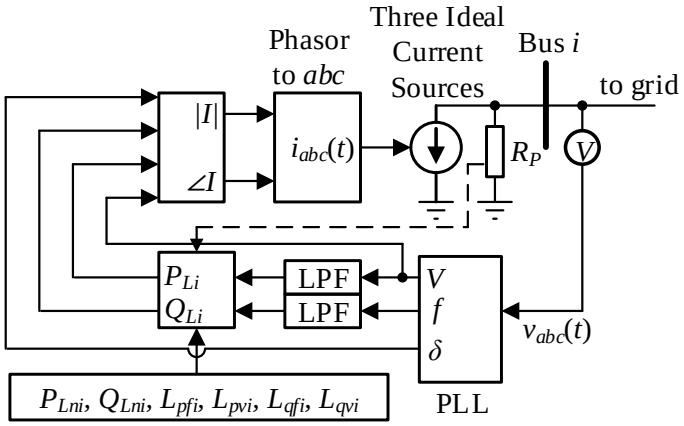

Fig. A2. Universal load model in TD simulation.

As shown in Fig. A2, a resistor is connected in parallel to the ideal current source. Using this resistor is inevitable in this type of load modeling when the grid lines are inductive-resistive; since without this resistor, the current source will be connected in series with the line inductor, which violates the circuit rules (continuity of inductor

currents). However, when this parallel part is added to the model, it will use an amount of active power, which is undesirable and decreases the model accuracy. For eliminating the resistor's effect on the total power, the total consumed power of the load should be reduced from the P_{Li}; a dashed line shows this correction in the model.

Appendix B. Specifications of DGs in different test systems

Table A1. DGs set-points and their droop characteristics for the 7-bus test system

	f_0	V_{01}, V_{03}	m_1, m_3	n_1, n_3	V_{02}	m_2	n_2
Case 1	1.02	1.00	0.0800	0.3227	1.00	0.0400	0.1614
Case 2	1.00	1.00	0.0645	0.2000	1.00	0.0323	0.1000
Case 3	1.00	1.00	0.0400	0.2000	1.00	0.0200	0.1000
Case 4	1.00	1.00	0.0400, ∞	0.3227, ∞	1.00	0.0200	0.1614

Table A2. Droop characteristics, and the P limitations of DGs for the 33-bus test system [8].

Units	$P_{G,\max}$	m	n
DG1-DG4	1.5	0.0010	0.005
DG5	1.5	0.0015	0.015

Table A3. Droop characteristics of DGs, and their Q limitations for the 38-bus test system.

Units	$Q_{G,\max}$	Case 1 [5]		Case 2	
		m	n	m	n
DG1	0.9	5.102×10^{-3}	0.02	6.886×10^{-3}	0.0556
DG2	0.6	1.502×10^{-3}	0.03333	5.478×10^{-3}	0.0833
DG3	0.9	4.506×10^{-3}	0.02	6.886×10^{-3}	0.0556
DG4, DG5	0.3	2.253×10^{-3}	0.05	10.956×10^{-3}	0.1667

Table A4. Locations, droop characteristics, and the P limitations of DGs for the 118-bus test system.

Units	Location	$P_{G,\max}$	Case 1		Case 2		Case 3	
			m	n	m	n	m	n
DG1	Bus 1	1.2	0.0167	0.1345	0.0269	0.0833	0.0167	0.0833
DG2-DG5	Buses 27, 54, 77, 86	0.6	0.0333	0.2689	0.0538	0.1667	0.0333	0.1667
DG6	Bus 105	0.8	0.0250	0.2017	0.0403	0.1250	0.0250	0.1250

Table A5. Locations, droop characteristics, and the P limitations of DGs for the 1k5-bus test system.

Units	Location	$P_{G,\max}$	Case 1 [20]		Case 2, Case 5		Case 3		Case 4	
			m	n	m	n	m	n	m	n
DG1	Bus 914	1.4	0.0500	0.0500	0.0143	0.1153	0.0231	0.0714	0.0143	0.0714
DG2-DG6	Buses 37, 175, 197, 564, 599	0.8	0.0500	0.0500	0.0250	0.2017	0.0403	0.1250	0.0250	0.1250

References

[1] W. H. Kersting. Distribution System Modeling and Analysis. 2nd ed. Boca Raton, FL, USA: CRC Press, 2006

[2] F. Milano. Power System Modelling and Scripting. New York, NY, USA: Springer, 2010

[3] M. Tostado-Véliz, S. Kamel and F. Jurado. A Novel Family of Efficient Power-Flow Methods With High Convergence Rate Suitable for Large Realistic Power Systems. IEEE Systems Journal 2020; 15(1): 738-746. https://doi.org/10.1109/JSYST.2020.2980156

[4] M. Tostado-Véliz, S. Kamel and F. Jurado. Efficient and Reliable Power-Flow Solution Using Recursive Formula. IEEE Systems Journal 2020 (Accessed 16 July 2020). https://doi.org/10.1109/ JSYST.2020.3007704

[5] F. Mumtaz, M. H. Syed, M. Al Hosani; H. H. Zeineldin. A Novel Approach to Solve Power Flow for Islanded Microgrids Using Modified Newton Raphson With Droop Control of DG. IEEE Trans. Sustain. Energy 2016; 7(2): 493-503. https://doi.org/10.1109/TSTE.2015.2502482

[6] G. Díaz, J. Gómez-Aleixandre, and J. Coto. Direct Backward/Forward Sweep Algorithm for Solving Load Power Flows in AC Droop-Regulated Microgrids. IEEE Trans. Smart Grid 2016. 7(5): 2208-2217. https://doi.org/10.1109/TSG.2015.2478278

[7] M. E. Nassar, M. M. A. Salama. A novel branch-based power flow algorithm for islanded AC microgrids. Electric Power Systems Research 2017; 146: 51-62. https://doi.org/10.1016/j.epsr.2017.01.019

[8] F. Hameed, M. Al Hosani and H. H. Zeineldin. A Modified Backward/Forward Sweep Load Flow Method for Islanded Radial Microgrids. IEEE Trans. Smart Grid 2019; 10(1): 910-918. https://doi.org/10.1109/TSG.2017.2754551

[9] M. M. A. Abdelaziz et al. A Novel and Generalized Three-Phase Power Flow Algorithm for Islanded Microgrids Using a Newton Trust Region Method. IEEE Trans. Power Systems 2013; 28(1): 190-201. https://doi.org/10.1109/TPWRS.2012.2195785

[10] M. H. Moradi, V. H. Foroutan and M. Abedini. Power flow analysis in islanded Micro-Grids via modeling different operational modes of DGs: A review and a new approach. Renew. Sustain. Energy Rev. 2017; 69: 248-262. https://doi.org/10.1016/j.rser.2016.11.156

[11] M. Bayat, K. Sheshyekani, and A. Rezazadeh. A unified framework for participation of responsive end-user devices in voltage and frequency control of the smart grid. IEEE Trans. Power Systems 2015; 30(3): 1369-1379. https://doi.org/10.1109/ TPWRS.2014.2344133

[12] M. Bayat et al. Coordination of Distributed Energy Resources and Demand Response for Voltage and Frequency Support of MV Microgrids. IEEE Trans. Power Systems 2016; 31(2): 1506-1516. https://doi.org/10.1109/ TPWRS.2015.2434938

[13] F. Feng and P. Zhang. Enhanced Microgrid Power Flow Incorporating Hierarchical Control. IEEE Trans. Power Systems 2020; 35(3): 2463-2466. https://doi.org/10.1109/ TPWRS.2020.2972131

[14] A. A. Nazari et al. A decoupled extended power flow analysis based on Newton-Raphson method for islanded microgrids. Int. J. Elect. Power Energy Syst. 2020; 117. 105705. https://doi.org/10.1016/j.ijepes.2019.105705

[15] G. C. Kryonidis et al. Power Flow of Islanded AC Microgrids: Revisited. IEEE Trans. Smart Grid 2018; 9(4): 3903-3905. https://doi.org/10.1109/TSG.2018.2799480

[16] E. O. Kontis et al. Power Flow Analysis of Islanded AC Microgrids. In: 2019 IEEE Milan PowerTech, Milan, Italy, 2019: 1-6. https://doi.org/10.1109/PTC.2019.8810612

[17] A. Kumar, B. K. Jha, D. Singh, and R. K. Misra. Current injection-based Newton–Raphson power-flow algorithm for droop-based islanded microgrids. IET Gener. Transmiss. Distrib. 2019; 13(23): 5271-5283. https://doi.org/10.1049/iet-gtd.2019.0575

[18] A. Kumar et al. A Nested-Iterative Newton-Raphson based Power Flow Formulation for Droop-based Islanded Microgrids. Electric Power System Research 2020; 180. 106131. https://doi.org/10.1016/j.epsr.2019.106131

[19] S. Kamel, M. Abdel-Akher and F. Jurado. Improved NR current injection load flow using power mismatch representation of PV bus. Int. J. Elect. Power Energy Syst. 2013; 53: 64-68. https://doi.org/10.1016/j.ijepes.2013.03.039

[20] R. A. Jabr, I. Džafić, B. C. Pal. Compensation in Complex Variables for Microgrid Power Flow. IEEE Trans. Power Syst. 2018; 33(3): 3207-3209. https://doi.org/10.1109/TPWRS.2018.2816809

[21] M. Bayat, K. Ghaseminezhad, A. A. Ghadimi. An efficient iterative approach for power flow solution of droop-controlled islanded AC microgrids through conventional methods. Int. J. Elect. Power Energy Syst. 2021; 130. 106962. https://doi.org/10.1016/j.ijepes.2021.106962

[22] X. H. T. Pham. Power sharing strategy in islanded microgrids using improved droop control. Electric Power Systems Research 2020; 180 106164. https://doi.org/10.1016/j.epsr.2019.106164

[23] M. A. Allam, A. A. Hamad and M. Kazerani. A Generic Modeling and Power-Flow Analysis Approach for Isochronous and Droop-Controlled Microgrids. IEEE Trans. Power Systems 2018; 33(5): 5657-5670. https://doi.org/10.1109/TPWRS.2018.2820059

[24] P. Kundur. Power system stability and control. McGraw-Hill, 1994

[25] R. D. Zimmerman and C. E. Murillo-Sánchez. Matpower Optimal Scheduling Tool MOST 1.0 User's Manual. Power Systems Engineering Research Center (PSerc), 2016

[26] M. E. Baran and F. Wu. Network reconfiguration in distribution system for loss reduction and load balancing. IEEE Trans. Power Del. 1989; 4(2): 1401–1407. https://doi.org/10.1109/61.25627

[27] C. Concordia and S. Ihara. Load representation in power system stability studies. IEEE Trans. Power App. and Syst. 1982: 969-977. https://doi.org/10.1109/TPAS.1982.317163

[28] D. Shirmohammadi, H. W. Hong, A. Semlyen and G. X. Luo. A compensation-based power flow method for weakly meshed distribution and transmission networks. IEEE Trans. Power Systems. 1988; 3(2): 753-762., https://doi.org/10.1109/59.192932

[29] D. Zhang, Zh. Fu, and L. Zhang. An improved TS algorithm for loss-minimum reconfiguration in large-scale distribution systems. Electric Power Systems Research 2007; 77 (5-6): 685–694. https://doi.org/10.1016/j.epsr.2006.06.005

[30] B. Standard, Voltage characteristics of electricity supplied by public distribution networks, BS EN; 2007.

[31] P. Aree. Accurate initialization of islanded microgrid including induction motor load using unified power‐flow approach. Electrical Engineering 2021; 103: 3085–3096 https://doi.org/10.1007/s00202-021-01280-y